Interaction effects in a quantum simulation of classical magnetism with artificial gauge potential

Hui Cao,[1,2] Qiang Wang,[3] and Li-Bin Fu[1,4,*]

[1]*National Laboratory of Science and Technology on Computational Physics, Institute of Applied Physics and Computational Mathematics, Beijing 100088, China*

[2]*School of Physics, Beijing Institute of Technology, Beijing 100081, China*

[3]*Beijing Advanced Science and Innovation Center, Chinese Academy of Sciences, Beijing 100864, China*

[4]*HEDPS, Center for Applied Physics and Technology, Peking University, Beijing 100084, China*

(Received 18 March 2013; revised manuscript received 28 October 2013; published 14 January 2014)

We investigate the effects of atomic interaction and artificial gauge potential in a quantum simulation of classical magnetism via ultracold bosonic atoms in triple wells. The system can be mapped into a transverse-field spin chain with Ising interaction under a twisted boundary condition. It undergoes a phase transition from planar to three-dimensional spin configurations, similar to the para-to-antiferromagnetic phase transition in the transverse-field Ising model, and the artificial gauge potential can tune this phase transition. The phase diagram is obtained, including ferromagnetic and spiral phases, similar to those simulated in Struck *et al*. [Struck, Ölschläger, Targat, Soltan-Panahi, Eckardt, Lewenstein, Windpassinger, and Sengstock, Science **333**, 996 (2011)].

DOI: 10.1103/PhysRevA.89.013610 PACS number(s): 67.85.−d, 03.67.Ac, 75.10.Hk

I. INTRODUCTION

Quantum simulation is an essential approach that employs an easily realized and flexibly controlled quantum system to emulate other systems of interest that may be otherwise intractable [1,2]. Among the most widely adopted simulators is a cold-atom system in various configurations of optical and/or magnetic traps [3–6] because of its high degrees of cleanness and controllability. It plays an important role in the study of magnetism, including the antiferromagnetic Ising interaction [7], frustrated quantum antiferromagnetism [8,9], itinerant ferromagnetism [10], superexchange interaction [11,12], and transverse-field Ising model [13–15], to name a few.

Frustrated classical magnetism has also been simulated by ultracold atoms in an anisotropic triangular lattice [16]. With negligible atomic interaction and homogeneous filling, the atoms in each site serve as a classical planar spin, and a variety of magnetic phases have been simulated [16]. However, in the presence of interaction, atomic population imbalance may be induced and, accordingly, the spins take three-dimensional arrangements. Moreover, when an artificial gauge potential is created, ultracold atoms in a closed chain of wells "feel" a virtual magnetic field or, equivalently, one can incorporate this external magnetic field into the boundary condition and thus consider a field-free system under a twisted boundary condition [17,18]. With the atomic interaction and artificial gauge potential included, the system becomes much more complicated, which nevertheless gives rise to some phenomena with novel properties.

The rest of the paper is organized as follows. In Sec. II, we introduce the triple-well model with artificial gauge potential. We then discuss, in Sec. III, the phase transition of the system, including the spin configurations, energy levels, magnetization, and phase diagram, which are followed by a conclusion in Sec. IV.

II. MODEL

In this paper, we study ultracold bosonic atoms in triple wells to explore the effects of the atomic interaction and artificial gauge potential. To this end, we only should make an effort to introduce a "magnetic flux" for the atoms tunneling through the triple wells, since our model, if without this magnetic flux, is indeed the same as a plaquette of the triangular lattice realized in [16]. Recently, there has been a lot of research trying to propose and demonstrate schemes for the experimental realization of this magnetic flux in a plaquette [19–22]. Using these techniques, we therefore obtain a system of cold atoms in triple wells with a magnetic flux ϕ when the atoms tunnel in a plaquette. By a gauge transformation, each tunneling between two neighboring lattice sites can take the same phase, either $\phi/3$ or $-\phi/3$. In the tight-binding approximation, the system Hamiltonian can be written as

$$H = -J\sum_{i=1}^{3}(a_i^\dagger a_j e^{i\phi/3} + \text{H.c.}) + \frac{U_0}{2}\sum_{i=1}^{3} n_i(n_i-1), \quad (1)$$

where $j = (i+1)\text{mod}\,3 + 1$ (here and below, this relation between i and j is supposed), J denotes the tunneling coupling, and U_0 is the atomic on-site interaction. The operator $a_i(a_i^\dagger)$ annihilates (creates) an atom in the ith well, $n_i = a_i^\dagger a_i$ counts the atom number in the ith well, and the total atom number $N = \sum_{i=1}^{3} n_i$ is conserved. The system has a periodic boundary condition if viewed in the presence of an external magnetic field. However, by a set of local transformations, say, $a_1 \to a_1$, $a_2 \to a_2 e^{i\phi/3}$, $a_3 \to a_3 e^{2i\phi/3}$, it becomes field free but obtains a twisted boundary condition [17,18], as these transformations can eliminate the phases (i.e., the magnetic flux) in all of the complex tunneling couplings, except for those transitions between the first and third wells [23] where the phase becomes ϕ and which is called the twisted angle.

When the interaction is negligible and the artificial gauge potential is absent, i.e., $U_0 = 0$, $\phi = 0$, the system is in a superfluid state with energy $E = -nJ\sum_{\langle i,k\rangle}\cos(\theta_i - \theta_k)$, where $\theta_{i(k)}$ is the local phase of atoms in the $i(k)$th well, $\sum_{\langle i,k\rangle}$ denotes summation over pairs of nearest neighbors, and homogeneous

*lbfu@iapcm.ac.cn

filling is assumed, i.e., $n_i = n_k = n$. The energy can be rewritten as $E = -nJ\sum_{\langle i,k\rangle}\mathbf{S}_i\cdot\mathbf{S}_k$ by introducing a classical vector spin $\mathbf{S}_i = [\cos\theta_i, \sin\theta_i]$, and thus the system can be employed to simulate classical spin systems [16]. However, in the presence of interaction, the above method of mapping the system to classical planar spins is no longer feasible. In this case, we would like to introduce the spin operators through the Schwinger transformation, $S_{ix} = \frac{1}{2}(a_i^\dagger a_j + a_j^\dagger a_i)$, $S_{iy} = \frac{1}{2i}(a_i^\dagger a_j - a_j^\dagger a_i)$, and $S_{iz} = \frac{1}{2}(a_i^\dagger a_i - a_j^\dagger a_j)$. After omitting the trivial constants, the system Hamiltonian (1) reduces to

$$H = -2J\sum_{i=1}^{3}\left(S_{ix}\cos\frac{\phi}{3} - S_{iy}\sin\frac{\phi}{3}\right) - \frac{4U_0}{3}\sum_{i=1}^{3}S_{iz}S_{jz}. \tag{2}$$

The system can now be regarded as a chain of three large spins subject to a transverse magnetic field $\mathbf{B} = 2J(\cos\frac{\phi}{3}, -\sin\frac{\phi}{3}, 0)$, and the spins mutually interact antiferromagnetically in the z-axis direction for $U_0 < 0$ or ferromagnetically for $U_0 > 0$. This model in essence differs from, although it resembles, a transverse-field Ising model (TIM) owing to lack of the global rotational symmetry in the xy plane caused by the twisted boundary condition. It is well known that a TIM undergoes a second-order phase transition from paramagnetic to (anti-)ferromagnetic states [24]. In the following, we will show that our model undergoes a similar phase transition and obtain some different properties as well.

For large spins, i.e., large occupation numbers in each trap in the model (1), we can treat them well as classical spins using the mean-field approximation. With the spins $\mathbf{S}_i$ represented in spherical coordinates $(S_i, \vartheta_i, \varphi_i)$, i.e., $\mathbf{S}_i = S_i(\sin\vartheta_i\cos\varphi_i, \sin\vartheta_i\sin\varphi_i, \cos\vartheta_i)$, the system energy is then determined by

$$E = \sum_{i=1}^{3}\left[-2S_i\sin\vartheta_i\cos(\varphi_i + \phi/3) + \frac{4\tau}{3}S_iS_j\cos\vartheta_i\cos\vartheta_j\right], \tag{3}$$

under the constraints of twisted boundary conditions. Here, $\varphi_i = \arctan(S_{iy}/S_{ix})$, $\tau = -U_0N/J$, $JN(>0)$ is used to scale the energy and the classical spins $\mathbf{S}_i$ are renormalized by N. When $\tau = 0$ and $\phi/3 = l\pi$ (here and below, l is an integer), this model is equivalent to that in Ref. [16] with identical tunneling couplings. If l is even (odd), the tunneling coupling is positive (negative). For the identical tunneling coupling considered in this paper, the same three magnetic phases can be simulated through these two models.

III. PHASE TRANSITION

A. Spin configurations

To derive the stationary states, we just need to obtain the fixed points (FPs) of the classical system (3) through solving the equations $\partial E/\partial\mathbf{R} = 0$ under the twisted boundary condition, where $\mathbf{R} = \{S_1 - S_3, S_2 - S_1, \varphi_2, -\varphi_3\}$ is a complete set of variables describing the motion of the system. In Fig. 1, we plot the energy levels and spin configurations (SCs) in the ground states (GSs) with different spin-spin coupling strengths. In the absence of spin-spin coupling

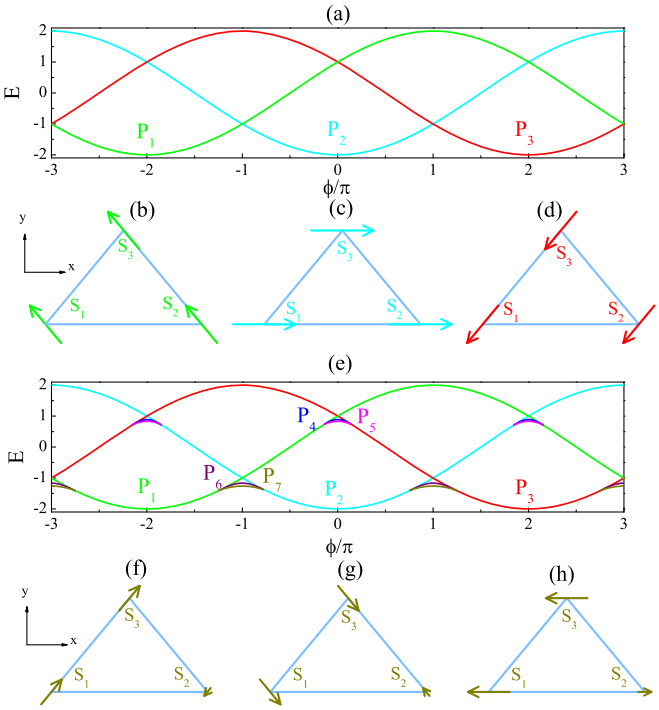

FIG. 1. (Color online) Mean-field energy levels and spin configurations (SCs) in the ground states for (a)–(d) $\tau = 0$ and (e)–(h) 2. P_{1-7} denote the fixed points. φ_i shows the direction of the spin $\mathbf{S}_i$ in the xy-plane projection. It represents the phase difference of atoms between two neighboring sites, other than the local phases used in Ref. [16]. (a) Energy levels for $\tau = 0$. (b)–(d) Planar SCs with all of the spins aligning parallel in the xy plane, (b) for $\phi \in (-3\pi, -\pi)$, $\varphi_i = 2\pi/3$; (c) for $\phi \in (-\pi, \pi)$, $\varphi_i = 0$; (d) for $\phi \in (\pi, 3\pi)$, $\varphi_i = -2\pi/3$. (e) Energy levels for $\tau = 2$. (f)–(h) Three-dimensional SCs with $S_{1z} = -S_{3z} \neq 0$ and $S_{2z} = 0$ for (f) $\phi = -\pi$, (g) $\phi = \pi$, and (h) $\phi = 3\pi$.

$(\tau = 0)$, all three stationary states display a planar and parallel magnetic order, in which the spins have the same magnitude and lie parallel in the xy plane: $S_1 = S_2 = S_3 = 1/3$, $\vartheta_1 = \vartheta_2 = \vartheta_3 = \pi/2$, $\varphi_1 = \varphi_2 = \varphi_3$. The variable φ_i actually characterizes the classical spins, similar to that proposed in Ref. [16]. However, here φ_i is denoted as the phase difference of atoms between two neighboring sites, other than the local phases themselves used in Ref. [16]. The direction of the spins is quantized due to the twisted boundary condition so that there exist only three SCs with $\varphi_i = 2\pi/3$, 0, and $-2\pi/3$, respectively [see Figs. 1(b)–1(d)]. These three configurations alternatively serve as the GS, depending on the twisted angle ϕ, with the energy $E = -2\cos(\varphi_i + \phi/3)$. Specifically, for $\phi \in (-3\pi, -\pi)$, $\varphi_i = 2\pi/3$ (FP P_1); for $\phi \in (-\pi, \pi)$, $\varphi_i = 0$ (FP P_2); and for $\phi \in (\pi, 3\pi)$, $\varphi_i = -2\pi/3$ (FP P_3). In this way, the spins follow the direction of the magnetic field $\mathbf{B}$ as close as possible so as to minimize the system energy.

For ferromagnetic spin-spin couplings ($\tau < 0$), the spins in the GS take the arrangements determined by ϕ just in the same way as in the case $\tau = 0$. However, for antiferromagnetic spin-spin interaction ($\tau > 0$), the magnetic order in the GS would undergo a transition from planar and parallel to three-dimensional arrangements. As an illustration, we show the energy levels and SCs with $\tau = 2$ in Figs. 1(e)–1(h). The

system obtains four more FPs in the vicinities of $\phi = l\pi$, with one of them (P_7) around $\phi = (2l+1)\pi$, instead of $P_{1,2,3}$, corresponding to the GS in which the spins take three-dimensional arrangements. In these SCs, two of the spins (here, for specification and without losing generality, we suppose they are $\mathbf{S}_1$ and $\mathbf{S}_3$) have the same magnitude, identical xy-plane projection, and reverse z-directional components, and the remaining spin ($\mathbf{S}_2$) stays in the xy plane. Specifically, for $\phi = (2l+1)\pi$ as in Figs. 1(f)–1(h), the xy-plane projections of $\mathbf{S}_1$ and $\mathbf{S}_3$ are parallel to the magnetic field, whereas $\mathbf{S}_2$ is antiparallel to it. As ϕ deviates from $(2l+1)\pi$, all of the spins deviate from the magnetic field direction and increase their xy-plane projections. Taking ϕ around π as an illustration, as ϕ decreases, the xy-plane projection of $\mathbf{S}_1$ ($\mathbf{S}_3$) rotates anticlockwise to approach the SC characterized by FP P_2, while $\mathbf{S}_2$ rotates clockwise; as ϕ increases, the spins would rotate in the opposite directions, respectively.

B. Energy levels and magnetization

To achieve an overall view of the energy-level structures, we show the dependence of the mean-field energy on the parameters τ and ϕ in Fig. 2. The FPs of the system can be grouped into two categories. One of them contains three FPs, $P_{1,2,3}$, denoting states with planar spins; the other group contains four FPs appearing in the vicinities of $\phi = l\pi$ [see Figs. 2(c), 2(e), 2(g)], in which all of the spins do not remain in the xy plane. In the latter group, the FPs appear in pair forming loop structures in the energy levels: a pair of them ($P_{4,5}$) first appears in the vicinities of $\phi = 2l\pi$ and another pair ($P_{6,7}$) appears in the vicinities of $\phi = (2l+1)\pi$. Whenever P_7 exists, it takes over the role of the GS. With $\tau = 2$ as an example, we can clearly see that the GS changes from P_2 to P_7, corresponding to the phase transition from planar to three-dimensional SC at $\phi_c = 2.36$ [see Fig. 2(c)]. As τ increases, the loop structures expand before they break at the critical points, i.e., $\tau_* = 13.46$ for $P_{4,5}$ and $\tau_* = 4$ for $P_{6,7}$. The FPs then exist for every single choice of ϕ. For quite large interaction strengths compared to these critical values, the energies of the FPs hardly depend on the parameter ϕ. As

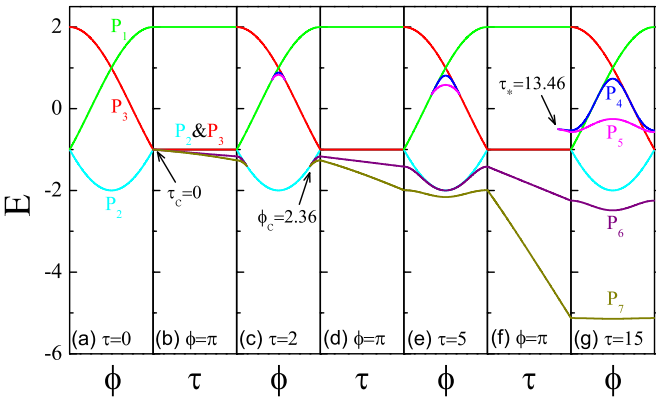

FIG. 2. (Color online) τ and ϕ dependence of the energy E. For any fixed τ, ϕ changes from $-\pi$ to π; in between, $\phi = \pi$ and τ changes linearly to the next fixed value. If the interaction is inverted ($\tau \to -\tau$), the energy levels would simply turn upside down and attain a shift of 3π in ϕ ($E \to -E, \phi \to \phi + 3\pi$).

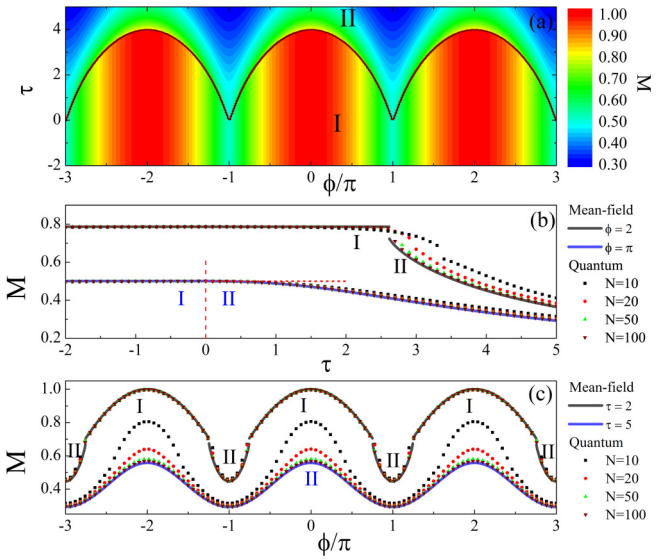

FIG. 3. (Color online) Phase diagram and magnetization. (a) Phase diagram and contour plot of the magnetization M. The phases I and II denote planar and three-dimensional spin configurations, respectively. (b),(c) Magnetization M as an order parameter. The solid lines denote the mean-field results. The dots denote the exact diagonalization results for different particle number, $N = 10, 20, 50, 100$. The vertical dashed line in (b) indicates the transition point at $\tau = 0$, and the horizontal one helps to show how the magnetization changes at the vicinity of the transition point. In phase I, M is constant against τ, while in phase II, M decreases with increasing τ.

for fixed ϕ, the system also undergoes a transition as τ varies. Particularly, for $\phi = (2l+1)\pi$ [see Figs. 2(b), 2(d), 2(f)], the emergence of FP P_7 at $\tau = 0$ indicates that the phase transition can take place with an infinitely small antiferromagnetic spin-spin coupling.

Based on the FP analysis above, the phase diagram can be constructed as in Fig. 3(a). The (ϕ, τ)-parameter space is divided into two regions, I and II, corresponding to the planar and three-dimensional SCs, respectively. For nonpositive τ, the system in the GSs always has planar spins. When τ is positive and small, there emerges a series of "windows" with ϕ in the vicinities of $(2l+1)\pi$, where the spin-spin coupling can drive the spins to have three-dimensional arrangements. As τ increases, these windows open wider and wider. On exceeding the critical value $\tau_c|_{\phi=2l\pi} = 4$, the windows merge together and the spins have three-dimensional arrangements for all of the directions of the magnetic field in the xy plane.

In Fig. 3(a), we also plot the contours of the magnetization $M = \sum_{i=1}^{3} \mathbf{S}_i \cdot \mathbf{B}/|\mathbf{B}|$, which shows clearly different behaviors in the two parameter regions. For a given ϕ, when τ is smaller than the critical value $\tau_c(\phi)$, the spins remain in configuration I and, consequently, the magnetization does not vary with respect to τ; when τ exceeds the critical value, the spins change to configuration II, thereby gradually reducing the magnetization as τ increases. For $\phi \neq (2l+1)\pi$, the magnetization is discontinuous at the critical value [see Fig. 3(b)]. As ϕ approaches $(2l+1)\pi$, this magnetization "gap" gradually decreases to zero. For $\phi = (2l+1)\pi$, the magnetization

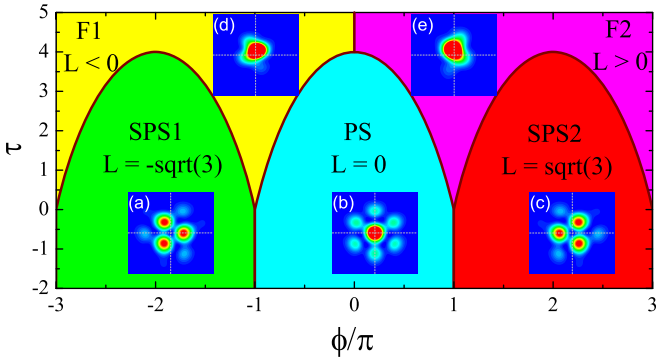

FIG. 4. (Color online) Whole phase diagram. The phase diagram is composed of five subphases, distinguished by the angular momentum L. F1 and F2 are two frustrated phases, SPS1 and SPS2 are two spiral planar spin phases, and PS is the planar spin phase. Insets: Numerical simulation of the time-of-flight (TOF) images by first obtaining the GSs of the system in the trapping potential, then letting the condensates expand freely, and, finally, recording the density patterns after a certain time duration. (a)–(c) Configurations I with $\tau = 1$ and (a) $\phi \in (-3\pi,-\pi)$, (b) $\phi \in (-\pi,\pi)$, and (c) $\phi \in (\pi,3\pi)$; (d),(e) configurations II with $\tau = 5$ and (d) $\phi = -\pi$, (e) $\phi = \pi$, respectively.

transition becomes continuous and the magnetization begins to decrease at $\tau = 0$. As for fixed τ between $\tau_c|_{\phi=(2l+1)\pi} = 0$ and $\tau_c|_{\phi=2l\pi} = 4$, the magnetization experiences several jumps and falls as the SCs switch between I and II [see Fig. 3(c)]. In Figs. 3(b) and 3(c), we also plot the exact diagonalization result of the magnetization with several particle numbers, $N = 10, 20, 50$, and 100. As the particle number increases, the exact diagonalization results gradually approach those from the mean-field methods.

C. Phase diagram

To experimentally spot different phases in Fig. 3, one can release the atoms from the confinement and record the time-of-flight (TOF) images. Here we plot in Fig. 4 the numerical simulation of the TOF images for several typical parameters. For configurations I, the patterns contain a symmetry of rotation $\pm 2\pi/3$ with respect to its center, while for configurations II, the patterns apparently lose this symmetry. In addition, it is clear that even in the same configuration, the TOF images also bear some apparent differences between each other, which can be quantitatively identified by the angular moment $L = -2\sum_i S_{iy}$ of the atomic condensate. For configurations I, the angular moment L is a constant, indicating the formation of vortices in the atomic condensates. Specifically, phase I contains three subphases with $L = -\sqrt{3}$ in Fig. 4(a) for the type-1 spiral planar spin (SPS1) phase, $L = 0$ in Fig. 4(b) for the planar spin (PS) phase, and $L = \sqrt{3}$ in Fig. 4(c) for the type-2 spiral planar spin (SPS2) phase. These three phases were also simulated in Ref. [16]. In contrast, L in configurations II changes with τ and ϕ. These states are indeed frustrated due to the interplay between the antiferromagnetic interaction and the triangular geometry. Similarly, phase II contains two subphases with negative (F1) and positive (F2) angular momenta, respectively. Thus, we derive the whole phase diagram comprising five subphases summarized in Fig. 4.

IV. CONCLUSION

To sum up, we have investigated the ground-state properties of ultracold bosonic atoms in triple wells, focusing, however, on the effects of atomic interaction and artificial gauge potential in a quantum simulation of classical magnetism. The system undergoes a phase transition from planar spin configurations containing the ferromagnetic phases and spiral phases similar to those simulated in [16] to three-dimensional configurations containing frustrated phases. All of the above results can be demonstrated experimentally with the present techniques. Starting from a triangular lattice, one should superpose a ring potential to "cut" a triple-well potential, tune the atomic interaction through Feshbach resonance, and, of course, use a set of laser configurations [20,21] or shake the trapping potential [22] to introduce the "magnetic flux." For the experiment in [16], i.e., $\phi = 0$, the actual interaction strength $|U_0|$ is much less than $4J$, i.e., $\tau \ll 4$, and thus we can ignore the atomic interaction and consider the spin to be planar.

ACKNOWLEDGMENTS

We are grateful to Hong Y. Ling for fruitful discussions. This work is supported by the National Fundamental Research Program of China (Contracts No. 2013CBA01502, No. 2011CB921503, and No. 2013CB834100) and the National Natural Science Foundation of China (Contracts No. 11374040, No. 11075020, and No. 11274051).

[1] R. Feynman, Int. J. Theor. Phys. **21**, 467 (1982).
[2] I. Buluta and F. Nori, Science **326**, 108 (2009).
[3] D. Jaksch and P. Zoller, Ann. Phys. **315**, 52 (2005).
[4] M. Lewenstein, A. Sanpera, V. Ahufinager, B. Damski, A. Sen(De), and U. Sen, Adv. Phys. **56**, 243 (2007).
[5] I. Bloch, Science **319**, 1202 (2008).
[6] I. Bloch, J. Dalibard, and S. Nascimbéne, Nat. Phys. **8**, 267 (2012).
[7] J. Simon, W. S. Bakr, R. Ma, M. E. Tai, P. M. Preiss, and M. Greiner, Nature (London) **472**, 307 (2011).
[8] A. Eckardt, P. Hauke, P. Soltan-Panahi, C. Becker, K. Sengstock, and M. Lewenstein, Europhys. Lett. **89**, 10010 (2010).
[9] Z.-X. Chen, H. Ma, M.-H. Chen, X.-F. Zhou, L. He, G.-C. Guo, X. Zhou, Y. Chen, and Z.-W. Zhou, Phys. Rev. A **85**, 013632 (2012).
[10] G.-B. Jo, Y.-R. Lee, J.-H. Choi, C. A. Christensen, T. H. Kim, J. H. Thywissen, D. E. Pritchard, and W. Ketterle, Science **325**, 1521 (2009).
[11] L.-M. Duan, E. Demler, and M. D. Lukin, Phys. Rev. Lett. **91**, 090402 (2003).

[12] S. Trotzky, P. Cheinet, S. Fölling, M. Feld, U. Schnorrberger, A. M. Rey, A. Polkovnikov, E. A. Demler, M. D. Lukin, and I. Bloch, Science **319**, 295 (2008).

[13] K. Kim, M.-S. Chang, S. Korenblit, R. Islam, E. E. Edwards, J. K. Freericks, G.-D. Lin, L.-M. Duan, and C. Monroe, Nature (London) **465**, 590 (2010).

[14] E. E. Edwards, S. Korenblit, K. Kim, R. Islam, M.-S. Chang, J. K. Freericks, G.-D. Lin, L.-M. Duan, and C. Monroe, Phys. Rev. B **82**, 060412(R) (2010).

[15] J. W. Britton, B. C. Sawyer, A. C. Keith, C. C. J. Wang, J. K. Freericks, H. Uys, M. J. Biercuk, and J. J. Bollinger, Nature (London) **484**, 489 (2012).

[16] J. Struck, C. Ölschläger, R. L. Targat, P. Soltan-Panahi, A. Eckardt, M. Lewenstein, P. Windpassinger, and K. Sengstock, Science **333**, 996 (2011).

[17] S. Viefers, P. Koskinen, P. S. Deo, and M. Manninen, Physica E **21**, 1 (2004).

[18] B.-B. Wei, S.-J. Gu, and H.-Q. Lin, J. Phys.: Condens. Matter **20**, 395209 (2008).

[19] J. Dalibard, F. Gerbier, G. Juzeliūnas, and P. Öhberg, Rev. Mod. Phys. **83**, 1523 (2011).

[20] Y.-J. Lin, R. L. Compton, K. Jiménez-García, J. V. Porto, and I. B. Spielman, Nature (London) **462**, 628 (2009).

[21] G. Juzeliūnas, J. Ruseckas, P. Öhberg, and M. Fleischhauer, Phys. Rev. A **73**, 025602 (2006).

[22] J. Struck, C. Ölschläger, M. Weinberg, P. Hauke, J. Simonet, A. Eckardt, M. Lewenstein, K. Sengstock, and P. Windpassinger, Phys. Rev. Lett. **108**, 225304 (2012).

[23] After the local transformation proposed in the text, the system Hamiltonian can be rewritten as $H = -J(a_2^\dagger a_1 + a_3^\dagger a_2 + a_1^\dagger a_3 e^{i\phi} + \text{H.c.}) + \frac{U_0}{2}\sum_{i=1}^{3} n_i(n_i - 1)$. It is evident that ϕ has a period of 2π. In fact, one can choose other local transformations to eliminate the phases in the complex coupling elements between the first and third wells while retaining others. However, by no means could all of the phases in the complex tunneling couplings be removed simultaneously only through local transformations.

[24] R. B. Stinchcombe, J. Phys. C **6**, 2459 (1973).